ACS EARTH AND SPACE CHEMISTRY

Article

Cite This: ACS Earth Space Chem. 2020, 4, 183−188

Pressure-Induced Hydration and Formation of Bilayer Ice in Nacrite, a Kaolin-Group Clay

Huijeong Hwang,[†] Jinhyuk Choi,[†] Zhenxian Liu,[‡] Duck-Young Kim,[§] Yu He,[§] Aaron J. Celestian,[∥] Thomas Vogt,[⊥] and Yongjae Lee*[,†,§]

[†]Department of Earth System Sciences, Yonsei University, Seoul 03722, Korea

[‡]Department of Civil and Environmental Engineering, The George Washington University, Washington, District of Columbia 20052, United States

[§]Center for High Pressure Science & Technology Advanced Research (HPSTAR), Shanghai 201203, China

[∥]Mineral Sciences, Natural History Museum of Los Angeles County, Los Angeles, California 90007, United States

[⊥]Nano Center and Department of Chemistry & Biochemistry, University of South Carolina, Columbia, South Carolina 29208, United States

Supporting Information

ABSTRACT: Pressure-induced hydration of the clay mineral nacrite, $Al_2Si_2O_5(OH)_4$ is, in contrast to its polymorph kaolinite, partially irreversible. At ambient conditions after pressure release, a majority phase with composition $Al_2Si_2O_5(OH)_4{\cdot}2H_2O$ with an intense (002) diffraction peak near $d \sim 8.4$ Å has been found. Both in situ X-ray diffraction and simulations based on the density functional theory point to intercalation of molecules in nominally nonswelling clays and specific geophysical and geochemical conditions.

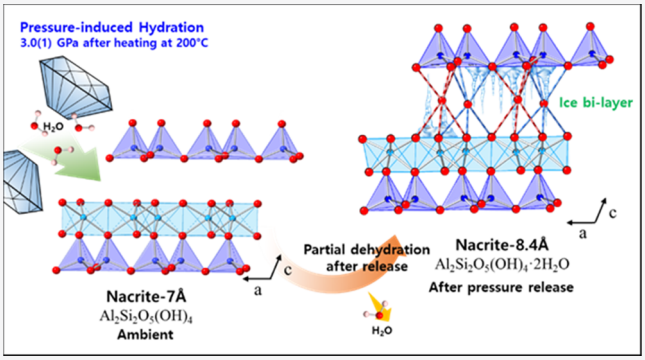

KEYWORDS: *pressure-induced hydration, clay minerals, kaolin-group minerals, nacrite, bilayer ice*

1. INTRODUCTION

Clay minerals are layered materials and comprise some of the most common materials on the Earth's surface.[1] Insertion of cations and molecules allows clay minerals to play an important role in industrial applications, such as the storage of nuclear waste and catalytic conversions of carbon dioxide.[1,2] Hydration and dehydration of clay minerals are of particular importance in geological processes, where they can impact fault line strength due to changes of lubricating properties.[3−6] Pressure-induced hydration (PIH), established in graphite oxide[7] and zeolites,[8,9] was also observed in synthetic smectite by You et al. (2013).[10] This study establishes partial irreversible PIH swelling in nacrite that is distinct from the established reversible PIH in kaolinite. Hwang et al. found that direct pressure- and heat-induced water insertion without the use of an organic solvent occurs at 2.5 GPa and 200 °C in kaolinite, the most abundant 1:1 phyllosilicate on Earth.[11] They characterized a new hydrated form of a clay mineral, superhydrated kaolinite, that is the most hydrated silicate mineral on Earth with ca. 17.3 wt % water. It should be noted that the discrepancies in quoted water content of clays in the kaolin group are rooted in the difference between containing molecular water as in $Al_2Si_2O_5(OH)_4{\cdot}nH_2O$ (i.e., $n = 2$ for halloysite, $n = 3$ for superhydrated kaolinite) or the loss of water during dehydroxylation in kaolinite and the formation of amorphous metakaolin according to $Al_2Si_2O_5(OH)_4 \rightarrow Al_2Si_2O_7 + 2H_2O$. Building on these studies, we anticipated pressure-induced water/molecular insertion in other clay minerals known as "nonswelling clays", such as polymorphs of kaolinite, serpentine-group minerals, and hydroxide minerals, which have strong hydrogen bonds between their layers.[12]

Nacrite is a naturally occurring rare polymorph of kaolinite with an ideal chemical composition $Al_2Si_2O_5(OH)_4$, which occurs in hydrothermal systems.[13] The transition kaolinite-to-dickite-to-nacrite with increasing temperature is well-documented in hydrothermal deposits using isotope methods.[14] A structural model for nacrite was first given by Gruner using X-ray powder diffraction.[15] Since Gruner's report other studies added to a more detailed structural model of nacrite.[16−18] The structure of nacrite is built up of one silica tetrahedral layer and

Received: September 29, 2019
Revised: November 7, 2019
Accepted: December 24, 2019
Published: December 24, 2019

DOI: 10.1021/acsearthspacechem.9b00255
ACS Earth Space Chem. 2020, 4, 183−188

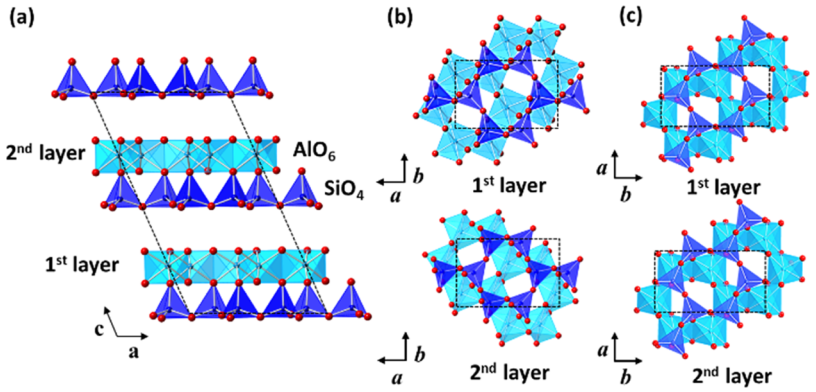

Figure 1. Crystal structure model of nacrite viewed along the (a) *b*-axis and (b) *c*-axis.[18] (c) The structural model of kaolinite is viewed along the *c*-axis for comparison.[19]

one alumina octahedral layer connected by oxygen. A repeat unit of two such layers describes the unit cell of nacrite (Figure 1).[19] The different orientation of hydroxyl groups causes a stacking order difference between kaolinite and nacrite. The second layer of kaolinite is shifted by $-a/3$ in reference to the first layer. On the other hand, the second layer of nacrite is rotated with respect to the first layer by 60°.[20] High-pressure-induced solid-to-solid transitions do not allow transitions between kaolinite and nacrite, as they would have to be reconstructive and not displacive. We have no indications for a dissolution−recrystallization mechanism between different members of the kaolin group.

In this paper, we report in situ high-pressure synchrotron X-ray powder diffraction experiments on nacrite up to 6.7(1) GPa in a diamond-anvil cell (DAC), which was also heated to promote phase transitions, to observe pressure- and temperature-induced changes of nacrite in the presence of water. Furthermore, we use in situ high-pressure infrared spectroscopy and ab initio random structure searching (AIRSS) based on the density functional theory (DFT) to corroborate the structural results.

2. EXPERIMENTAL METHODS

2.1. Sample Preparation. In situ high-pressure synchrotron X-ray diffraction powder experiments were performed using a symmetric-type diamond-anvil cell (DAC) with diamonds having culets measuring 500 μm in diameter. Natural nacrite from Schweighausen, Germany (Natural History Museum of Los Angeles County #22873) was loaded into the sample chamber with 235 μm diameter and 70 μm height drilled by electrospark erosion of a stainless-steel gasket. To determine the sample chamber pressure, small ruby spheres were added into the sample chamber together with the nacrite powder. The pressure of the sample after compression was determined by the shift of the R1 emission line (precision: 0.1 GPa).[21] After sample loading, we put the pressure-transmitting medium (PTM) into the sample chamber. We used silicone oil as a nonpore penetrating PTM and water as a pore-penetrating PTM.

2.2. In Situ High-Pressure Synchrotron X-ray Powder Diffraction. We measured the in situ high-pressure synchrotron X-ray powder diffraction data of nacrite at beamline 6D in the Pohang Accelerator Laboratory (PAL) and beamline 10−2 at the Stanford Synchrotron Radiation Lightsource (SSRL) at the SLAC National Accelerator Laboratory. At beamline 6D at PAL, we collected in situ high-pressure synchrotron X-ray powder diffraction data for nacrite in the presence of silicone oil. The primary white beam from the bending magnet source at beamline 6D at PAL was monochromated using Si(111) double crystals providing a wavelength of 0.653(1) Å. The powder diffraction data were collected using a CCD detector (Reyonix-MX225HS) with a 240 mm sample-to-detector distance to cover a 2θ range up to 35°. The in situ high-pressure synchrotron X-ray powder diffraction data for nacrite with water were collected at beamline 10−2 at SSRL. At beamline 10−2 located near a wiggler, the monochromatic X-ray beam from a Si(220) plane gave a wavelength of 0.620(1) Å. At this beamline, we used the Pilatus 300K-w Si-diode CMOS detector to collect powder diffraction data at a 1210 mm sample-to-detector distance with 2θ coverage up to 30°. The pressure was increased up to 7.0(1) GPa in intervals of about 0.5−1.0 GPa. The sample equilibrated for about 10 min in the DAC at each measured pressure. To ensure a homogeneous phase transition, ex situ heating was done by placing the sample containing water in a DAC inside an oven at 200 °C for 1 h.

Pressure-dependent changes in the lattice parameters and unit-cell volumes were derived by whole-pattern profile fitting using the Le Bail method implemented in the GSAS suite of programs.[22] The background curve was fitted using a Chebyshev polynomial with <30 coefficients. The pseudo-Voigt profile function proposed by Thompson and colleagues was used to model the observed Bragg reflection.[23] Bulk moduli from normalized volume (V/V_0) were calculated using the second-order Birch−Murnaghan equation of state (EOS).[24] The structural model of nacrite-8.4 Å after the pressure release was established by Rietveld methods.[25]

2.3. In Situ High-Pressure Synchrotron Infrared Spectroscopy. High-pressure IR experiments were performed at the beamline 22-IR-1 of the NSLS-II at Brookhaven National Laboratory. To avoid absorption saturation from the water present, all IR spectra were collected in reflection mode using a Bruker Vertex 80v FTIR spectrometer and a Hyperion 2000 IR microscope equipped with a liquid nitrogen-cooled midband MCT detector. A DAC containing a pair of type-II diamond anvils with 500 μm culet size was used. The ruby fluorescence technique was utilized to estimate the pressures for all experiments at room temperature. Nacrite with water was loaded into a 235 μm wide and 70 μm thick sample chamber drilled using electrospark erosion in a preindented stainless-steel gasket. Near the edge of the chamber, a few small ruby spheres (~20 μm) were added as pressure gauges.

DOI: 10.1021/acsearthspacechem.9b00255
ACS Earth Space Chem. 2020, 4, 183−188

The reflectance from the sample−diamond interface ($R_{sd}(\omega)$) is calculated using

$$R_{sd} = I_{sd}I_d/I_eI_0$$

where R_{sd} is the reflectivity of the sample−diamond interface, I_{sd} the intensity reflected from the sample−diamond interface, I_d the intensity reflected from the air−diamond interface, I_e the intensity reflected from the empty cell, and I_0 the intensity reflected from the gold foil.[26] Although it is impossible to obtain accurate R_{sd} values due to both sample and water being present, our goal was to monitor the changes in the O−H stretching vibrational modes. The changes in the frequencies of the O−H stretching vibrational modes are related to the structural changes that occur during the insertion of the H_2O molecules between the layers in the nacrite structure.

2.4. Rietveld Refinement. The Rietveld refinement program in the EXPGUI suite was used for structural characterization of the hydrated nacrite after pressure release.[22,27] The background curve and peak shape were modeled using the Le Bail method. These values were used as starting parameters for the Rietveld refinement and allowed to vary subsequently. The starting model of the structure of hydrated nacrite was the one proposed by Amara et al. (1998).[28] After initial refinements, an inspection of difference-Fourier maps suggested two interlayer sites showing residual electron densities, which were subsequently modeled as oxygen atoms of H_2O molecules: OW1 at (0.290(1), 0.119(2), and 0.380(8)) and OW2 at (0.609(1), 0.173(2), and 0.365(8)). The refined occupancies of the OW1 and OW2 sites converged to 1. Geometrical soft restraints were applied for the layer interatomic distances assuming ideal tetrahedral and octahedral geometries, that is, Si−O = 1.610(1) Å and O−O = 2.630(5) Å for SiO_4 and Al−O = 1.885(1) Å and O−O = 2.668(5) Å for AlO_6. Isotropic displacement parameters (U_{iso}) were grouped to be the same or for the same atoms to reduce the number of parameters. The final convergence of the refinement was achieved by simultaneously varying all of the background and profile parameters, preferred orientation parameters, scale factor, lattice constants, 2θ zero, and the atomic positional and displacement parameters. The parameters of the final refined models are listed in Supporting Information Tables S2 and S4.

2.5. Computational Results. *2.5.1. AIRSS.* To predict the atomic configuration of superhydrated nacrite, we conducted crystal structure searches based on Ab Initio Random Structure Searching (AIRSS)[29] combined with the standard density functional theory-based software VASP.[30] To determine computationally the atomic positions of inserted water molecules, we fixed the atomic positions of the nacrite layers of a 1 × 2 × 1 supercell (16 formula units) constraining the interlayer distance to 8.4 Å and only conducted random structure searches for the inserted water molecules between the layers. We allowed for the full relaxation of atomic positions. Figure S3 shows the ground state atomic positions out of ∼1000 trial configurations.

2.5.2. Equations of State. Using the predicted crystal structure of recovered superhydrated nacrite, we extracted the total energy versus volume relationship. In our calculations, the local density approximation pseudopotential with a cutoff energy of 1000 eV was used. A *k*-point mesh with a spacing of ca. 0.03 $Å^{-1}$ was adopted. Geometry optimizations were performed at various constant volumes by using a conjugate gradient minimization until all of the forces acting on ions were less than 0.01 eV/Å per atom. The calculated energy−volume data were fitted to a third-order Birch−Murnaghan equation of state (EOS)

$$E(V) = E_0 + \frac{9V_0B_0}{16}\left\{\left[\left(\frac{V_0}{V}\right)^{2/3} - 1\right]^3 B_0' + \left[\left(\frac{V_0}{V}\right)^{2/3} - 1\right]^2 \left[6 - 4\left(\frac{V_0}{V}\right)^{2/3}\right]\right\} \quad (1)$$

where E_0 denotes the intrinsic energy at zero pressure, V_0 is the volume at zero pressure, B_0 is the bulk modulus, and B_0' the first pressure derivative of the bulk modulus. The relation between the pressure and the volume at zero Kelvin can be expressed as

$$P(V) = \frac{3B_0}{2}\left[\left(\frac{V_0}{V}\right)^{7/3} - \left(\frac{V_0}{V}\right)^{5/3}\right]\left\{1 + \frac{3}{4}(B_0' - 4)\left[\left(\frac{V_0}{V}\right)^{2/3} - 1\right]\right\} \quad (2)$$

3. RESULTS AND DISCUSSION

Pressure-dependent changes in the measured synchrotron powder X-ray diffraction of nacrite are shown as a function of pressure in Figure 2. The *d*-spacing of the (002) plane near 7 Å, the distance between layers along the direction of stacked layers, initially contracts in comparison to the *a*- and *b*-axes when going up to pressures of 1.8(1) GPa. This initial behavior establishes the intrinsic pressure-dependent anisotropic compression in nacrite, similar to what was observed in other clay minerals, such as smectite and kaolinite.[31,32]

At 3.0(1) GPa, after heating the diamond-anvil cell at 200 °C for 1 h in an oven, the synchrotron powder X-ray diffraction pattern reveals the appearance of a new reflection with a *d*-spacing near ∼10 Å. Further annealing near 3 GPa increases the intensity of this new reflection, but further pressure increases up to 6.6(1) GPa decreases it again. This new PIH-expanded phase is stable up to 6.6(1) GPa and down to 1.4(1) GPa during decompression. As nacrite is a polymorph of kaolinite, we posit that this phase is $Al_2Si_2O_5(OH)_4{\cdot}3H_2O$, containing, as superhydrated kaolinite, 3 water molecules per formula unit between the tetrahedral silica and octahedral alumina layers and having a water content of 17.3%. A detailed structural characterization requires us to take data with a larger *q*-range. During the PIH, the distance of the (002) plane increases by about 33%, while the lengths of the *a*- and *b*-axes continue to decrease. The corresponding expansion of the unit-cell volume is approximately 31%. The bulk modulus of the expanded phase of nacrite is K_0 = 40.6(1) GPa, which is smaller than that of the original nacrite (nacrite-7 Å) with K_0 = 49.5(3) GPa. To determine the bulk modulus of the latter phase, we undertook pressure experiments with silicone oil, which is a pressure-transmitting medium that does not intercalate between the nacrite layers. The results are shown in Figure S1.

After complete pressure release, the (002) reflection with *d*-spacing near 10 Å of the expanded nacrite disappears and a new reflection near ∼8.4 Å emerges as does a diffuse (002) reflection near ∼7 Å of the initial nacrite phase. This is

DOI: 10.1021/acsearthspacechem.9b00255
ACS Earth Space Chem. 2020, 4, 183−188

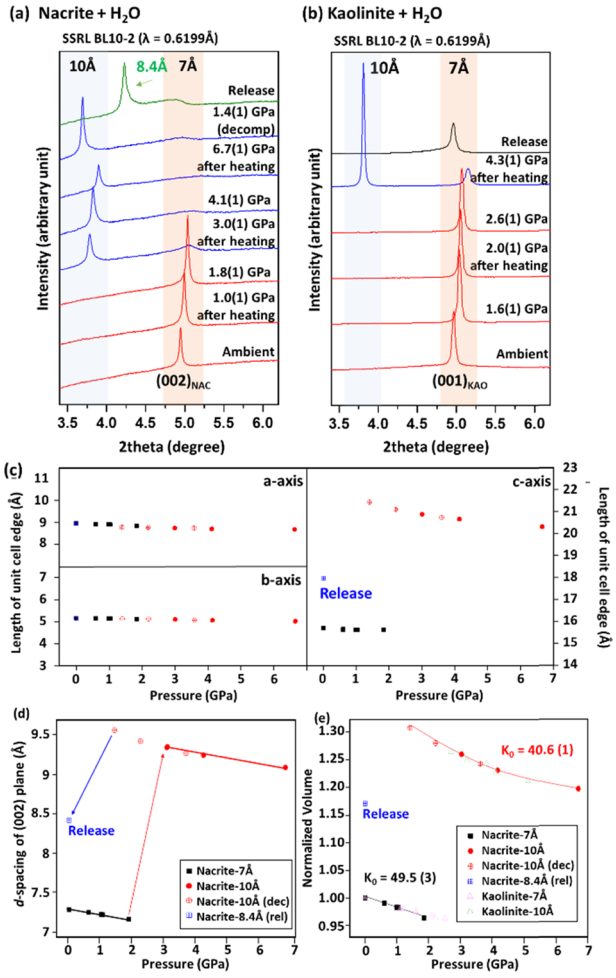

Figure 2. Synchrotron X-ray powder diffraction patterns of (a) nacrite and (b) kaolinite at ambient and high pressures, as well as annealed at different temperatures, in the presence of water as a pore-penetrating medium. Pressure-dependent changes in the (c) refined unit-cell parameters, (d) *d*-spacing of (002) reflection, and (e) normalized unit-cell volume for nacrite.

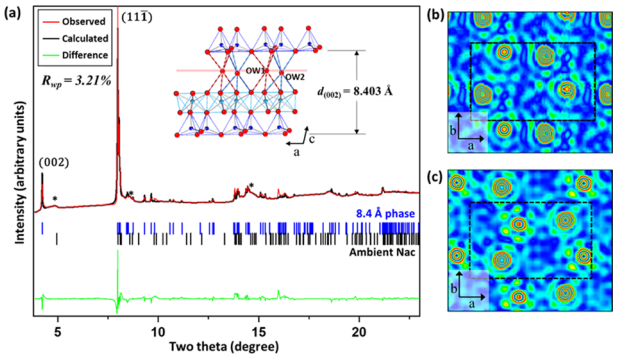

Figure 3. (a) Rietveld fit and refined structural model of the nacrite-8.4 Å phase measured at ambient conditions after pressure release. The calculated positions of the Bragg reflections of the nacrite-7 Å (ca. 8 wt %) and nacrite-8.4 Å (ca. 92 wt %) phases are shown by black and blue vertical bars, respectively, together with a difference curve in green from the two-phase refinement. (b) The calculated electron density map based on the refined structural model for the nacrite-8.4 Å phase shows the positions of oxygen atoms (H_2O molecules) in the interlayer plane. (c) The calculated electron density map of the DFT-simulated structural model for the nacrite-8.4 Å phase.

different to what is observed in superhydrated kaolinite, which shows a completely reversible PIH after pressure release.[11]

The structural model of the nacrite-8.4 Å phase was derived by Rietveld refinement of synchrotron X-ray powder diffraction data. The diffraction peaks of the nacrite-8.4 Å phase are indexed in space group *Cc* (no. 9), the same as the original nacrite-7 Å phase. Based on a starting structural model by Amara et al. (1998),[28] difference-Fourier synthesis displayed maxima of electron densities between the layers (Figure 3). Subsequent modeling and refining these electron densities using oxygen atoms of the H_2O molecules at two crystallographically distinct interlayer sites lead to a chemical composition of $Al_2Si_2O_5(OH)_4{\cdot}2H_2O$. Compared to the superhydrated kaolinite, which has three fully occupied interlayer H_2O sites, the recovered nacrite-8.4 Å phase is 71% superhydrated with a net water content of 12.2 wt %. The average interatomic distances between the oxygen of H_2O molecules and the framework oxygen in tetrahedral and octahedral layers are 2.84(1) and 2.82(1) Å, respectively, indicating strong hydrogen bonding.

To confirm the positions of water molecules in the nacrite-8.4 Å phase, we conducted a constraint structure prediction using Ab Initio Random Structure Searching (AIRSS)[29] combined with the first-principles software VASP[30] based on the density functional theory only for the inserted water molecules into pristine nacrite. Figure 3c shows the electron density map of the predicted crystal structure in the interlayer space, which gives an excellent agreement with the experimentally observed one. We also estimated the bulk moduli K_0 of nacrite-7 Å and nacrite-8.4 Å using a third-order Birch–Murnaghan equation of state (EOS), which yield 47.3 GPa and 34.5 GPa, respectively. These values show that the PIH-expanded nacrite is more compressible, which is consistent with the experimental results (Figure 2).

We find an important difference in the coordination environment of the pressure-inserted H_2O molecules in the recovered nacrite-8.4 Å phase and superhydrated kaolinite (Figure 4). The two interlayer H_2O oxygen atoms in nacrite-8.4 Å are both coordinated by six oxygen atoms of the tetrahedral and octahedral layers, in a configuration similar to that of ice Ih, whereas the interlayer H_2O coordination in the superhydrated kaolinite is either 2-fold or one coordinated, similar to that of bulk water. This might be related to the stability of the recovered nacrite-8.4 Å phase.

Hydroxyl vibrations of nacrite are indicators of changes in the interlayer hydrogen bonding and molecular intercalation. The formation and recovery of interlayer H_2O that is contained within the PIH structures of nacrite can be corroborated by infrared absorbance spectra measured at high pressure and after pressure release at ambient conditions. Figure S2 shows in situ high-pressure infrared spectra of nacrite in the presence of water. The positions of the OH vibrations in the region between 3600 and 3700 cm^{-1} shift to higher wavenumbers as the pressure increases up to 2.6(1) GPa. At 3.0(1) GPa after heating the sample at 250 °C, major changes are observed upon the formation of the PIH-expanded phase, e.g., a new stretching band appeared near 3560 cm^{-1}, which is characteristic of the interlayer H_2O molecules, similar to those observed in the superhydrated kaolinite, halloysite, and smectite.[11,33]

DOI: 10.1021/acsearthspacechem.9b00255
ACS Earth Space Chem. 2020, 4, 183–188

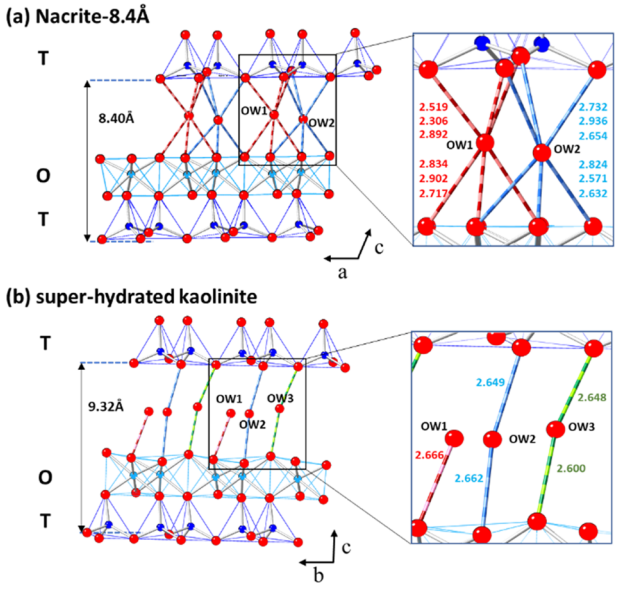

Figure 4. Comparison of the oxygen coordination environments for the interlayer H_2O between (a) nacrite-8.4 Å and (b) superhydrated kaolinite.[11]

Figure 5 compares the infrared spectrum of the original nacrite-7 Å and the recovered nacrite-8.4 Å phases. Nacrite-7 Å

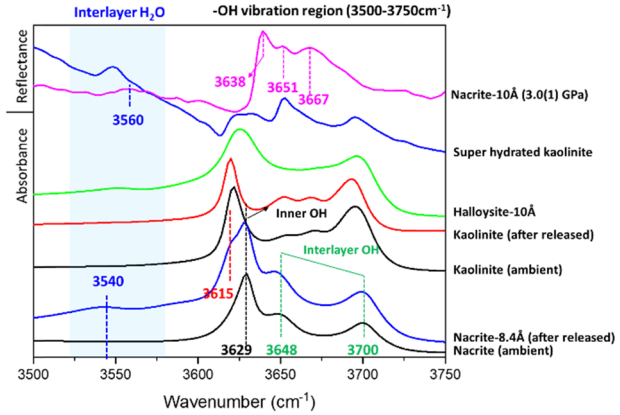

Figure 5. Infrared spectra of nacrite, nacrite-10 Å at 3.0(1) GPa, and nacrite-8.4 Å after pressure release, compared to the spectra from kaolinite, superhydrated kaolinite, recovered kaolinite after pressure release, and natural halloysite-10 Å.

has three characteristics hydroxyl (OH) vibrations at 3629, 3648, and 3700 cm^{-1}.[34] The hydroxyl vibration at 3629 cm^{-1} is assigned to one inner hydroxyl, while the other hydroxyl vibrations at the higher wavenumbers originate from the interlayer hydroxyls of nacrite-7 Å. In nacrite-8.4 Å at ambient conditions, two new stretching bands near 3540 and 3615 cm^{-1} are observed in addition to the three-stretching bands as observed in nacrite-7 Å. The new stretching band near 3540 cm^{-1} of nacrite-8.4 Å occurs due to the hydration of nacrite and is similar to what was observed in hydrated halloysite.[35] The other band near 3615 cm^{-1} is due to an OH stretching mode of H_2O located in the interlayer of nacrite-8.4 Å.[36] The infrared data of the nacrite-8.4 Å phase thus supports our refined crystallographic model and in particular the interlayer H_2O arrangement.

4. CONCLUSIONS

This study establishes that nacrite, a polymorph of kaolinite, behaves differently from kaolinite at high pressures and temperatures in the presence of water. In contrast to the completely reversible PIH observed in kaolinite, nacrite undergoes partially irreversible PIH upon pressure release and is therefore an important indicator for geophysical processes at elevated pressures and temperatures in the presence of water. X-ray diffraction data taken on Mars are often dominated at a low angle by diffraction at $d \sim 10$ and ~14 Å, which is indicative of phyllosilicates.[37] Spectroscopic measurements show the presence of hydrated kaolin minerals, such as halloysite, on the surface of Mars.[38,39] Most clay minerals can be grouped according to their strongest reflection being 7, 10, or 14 Å.[40] The observation of diffraction near 8.4 Å would therefore be a strong evidence of irreversible PIH as observed in nacrite and points to the P-T conditions of past geophysical processes. A better understanding of PIH in clay minerals and other phyllosilicates is important for unraveling geophysical processes on Earth and other planetary bodies, including if and how they alter the evolution of clay minerals.[40]

■ ASSOCIATED CONTENT

Supporting Information

The Supporting Information is available free of charge at https://pubs.acs.org/doi/10.1021/acsearthspacechem.9b00255.

In situ high-pressure synchrotron X-ray powder diffraction patterns measured on nacrite with silicone oil as the nonpenetrating pressure medium (Figure S1); in situ high-pressure synchrotron infrared reflectivity spectra of nacrite with water as a penetrating pressure medium during compression and heating (Figure S2); predicted crystalstructure of nacrite-8.4 Å (Figure S3); crystal data and details pertaining to the structure refinements of the original nacrite, nacrite-8.4 Å at ambient condition, and superhydrated kaolinite at 4.1 GPa (Table S1−S3) (PDF)

■ AUTHOR INFORMATION

Corresponding Author

*E-mail: yongjaelee@yonsei.ac.kr.

ORCID

Aaron J. Celestian: 0000-0003-0775-6380

Yongjae Lee: 0000-0002-2043-0804

Author Contributions

H.H. contributed to the experiments and data analysis with the help from J.C and Z.L. D.-Y.K. and Y.H. contributed to computational calculations. Y.L. designed the research, discussed the results with A.J.C. and T.V., and worked on the manuscript with all authors.

Notes

The authors declare no competing financial interest.

■ ACKNOWLEDGMENTS

This work was supported by the Leader Researcher program (NRF-2018R1A3B1052042) of the Korean Ministry of Science and ICT. We also thank the partial supports by NRF-2019K1A3A7A09033395 and NRF-2016K1A4A3914691 grants. Synchrotron experiments were performed at the beamlines 6D at PLS-II, BL10-2 at SSRL, and

DOI: 10.1021/acsearthspacechem.9b00255
ACS Earth Space Chem. 2020, 4, 183−188

22-IR-1 at NSLS-II. This research was partially supported by the Graduate School of YONSEI University Research Scholarship Grants in 2019.

REFERENCES

(1) Meunier, A. *Clays*; Springer: Berlin, 2005.
(2) Hansen, E. L.; Hemmen, H.; Fonseca, D. M.; Coutant, C.; Knudsen, K. D.; Plivelic, T. S.; Bonn, D.; Fossum, J. O. Swelling transition of a clay induced by heating. *Sci. Rep.* **2012**, *2*, No. 618.
(3) Carpenter, B. M.; Marone, C.; Saffer, D. M. Weakness of the San Andreas Fault revealed by samples from the active fault zone. *Nat. Geosci.* **2011**, *4*, 251−254.
(4) Van Der Pluijm, B. Natural fault lubricants. *Nat. Geosci.* **2011**, *4*, 217−218.
(5) Schleicher, A. M.; Hofmann, H.; Pluijm, B. V. Constraining clay hydration state and its role in active fault systems. *Geochem. Geophys. Geosyst.* **2013**, *14*, 1039−1052.
(6) Sánchez-Roa, C.; Vidal, O.; Jiménez-Millán, J.; Nieto, F.; Faulkner, D. R. Implications of sepiolite dehydration for earthquake nucleation in the Galera Fault Zone: A thermodynamic approach. *Appl. Geochem.* **2018**, *89*, 219−228.
(7) Talyzin, A. V.; Solozhenko, V. L.; Kurakevych, O. O.; Szabó, T.; Dékány, I.; Kurnosov, A.; Dmitriev, V. Colossal pressure-induced lattice expansion of graphite oxide in the presence of water. *Angew. Chem., Int. Ed.* **2008**, *47*, 8268−8271.
(8) Lee, Y.; Vogt, T.; Hriljac, J. A.; Parise, J. B.; Artioli, G. Pressure induced volume expansion of zeolites in the natrolite family. *J. Am. Chem. Soc.* **2002**, *124*, 5466−5475.
(9) Seoung, D.; Lee, Y.; Kao, C.-C.; Vogt, T.; Lee, Y. Two-step pressure-induced superhydration in small pore natrolite with divalent extra-framework cations. *Chem. Mater.* **2015**, *27*, 3874−3880.
(10) You, S.; Kunz, D.; Stöter, M.; Kalo, H.; Putz, B.; Breu, J.; Talyzin, A. V. Pressure-induced water insertion in synthetic clays. *Angew. Chem., Int. Ed.* **2013**, *52*, 3891−3895.
(11) Hwang, H.; Seoung, D.; Lee, Y.; Liu, Z.; Liermann, H.-P.; Cynn, H.; Vogt, T.; Kao, C.-C.; Mao, H.-K. A role for subducted super-hydrated kaolinite in Earth's deep water cycle. *Nat. Geosci.* **2017**, *10*, 947−953.
(12) Giese, R. F. The electrostatic interlayer forces of layer structure minerals. *Clays Clay Miner.* **1978**, *26*, 51−57.
(13) Buatier, M. D.; Potdevin, J.-L.; Lopez, M.; Petit, S. Occurrence of nacrite in the Lodève Permian basin (France). *Eur. J. Mineral.* **1996**, *8*, 847−852.
(14) Marumo, K. Genesis of kaolin minerals and pyrophyllite in Kuroko deposits of Japan: Implications for the origins of the hydrothermal fluids from mineralogical and stable isotope data. *Geochim. Cosmochim. Acta* **1989**, *53*, 2915−2924.
(15) Gruner, J. W. The crystal structure of nacrite and a comparison of certain optical properties of the kaolin group with its structures. *Z. Kristallogr. - Cryst. Mater.* **1933**, *85*, 345−354.
(16) Bailey, S. W. Polymorphism of the kaolin minerals. *Am. Mineral.* **1963**, *48*, 1196−1209.
(17) Blount, A. M.; Threadgold, J. M.; Bailey, S. W. Refinement of the crystal structure of nacrite. *Clays Clay Miner.* **1969**, *17*, 185−194.
(18) Zheng, H.; Bailey, S. W. Refinement of the nacrite structure. *Clays Clay Miner.* **1994**, *42*, 46−52.
(19) Bish, D. L.; Von Dreele, R. B. Rietveld refinement of non-hydrogen atomic positions in kaolinite. *Clays Clay Miner.* **1989**, *37*, 289−196.
(20) Bookin, A. S.; Drits, V. A.; Plancon, A.; Tchoubar, C. Stacking faults in kaolin-group minerals in the light of real structural features. *Clays Clay Miner.* **1989**, *37*, 297−307.
(21) Mao, H. K.; Xu, J.; Bell, P. M. Calibration of the ruby pressure gauge to 800-kbar under quasihydrostatic conditions. *J. Geophys. Res.* **1986**, *91*, 4673−4676.
(22) Toby, B. H. EXPGUI, a graphical user interface for GSAS. *J. Appl. Crystallogr.* **2001**, *34*, 210−213.
(23) Thompson, P.; Cox, D. E.; Hastings, J. B. Rietveld refinement of Debye−Scherrer synchrotron X-ray data from Al_2O_3. *J. Appl. Crystallogr.* **1987**, *20*, 79−83.
(24) Birch, F. Finite elastic strain of cubic crystals. *Phys. Rev.* **1947**, *71*, 809−824.
(25) Rietveld, H. M. A profile refinement method for nuclear and magnetic structures. *J. Appl. Crystallogr.* **1969**, *2*, 65−71.
(26) Seagle, C. T.; Heinz, D. L.; Liu, Z.; Hemley, R. J. Synchrotron infrared reflectivity measurements of iron at high pressures. *Appl. Opt.* **2009**, *48*, 545−552.
(27) Larson, A. C.; Von Dreele, R. B. *GSAS—General Structure Analysis System*; Los Alamos National Laboratory, 1986.
(28) Amara, A. B. H.; Brahim, J. B.; Plancon, A.; Ben rhaiem, H. Étude par Diffraction X des Modes d'Empilement de la Nacrite Hydratée et Deshydratée. *J. Appl. Crystallogr.* **1998**, *31*, 654−662.
(29) Pickard, C. J.; Needs, R. J. High-pressure phases of silane. *Phys. Rev. Lett.* **2006**, *97*, No. 045504.
(30) Kresse, G. Efficient iterative schemes for ab initio total-energy calculations using a plane-wave basis set. *Phys. Rev. B* **1996**, *54*, 11169−11186.
(31) Welch, M. D.; Crichton, W. A. Pressure-induced transformations in kaolinite. *Am. Mineral.* **2010**, *95*, 651−654.
(32) Voltolini, M.; Wenk, H.-R.; Mondol, N. H.; Bjørlykke, K.; Jahren, J. Anisotropy of experimentally compressed kaolinite-illite-quartz mixtures. *Geophysics* **2009**, *74*, D13−D23.
(33) Wilson, M. J. *Clay Mineralogy: Spectroscopic and Chemical Determinative Methods*; Chapman & Hall: London, 1994.
(34) Farmer, V. C. *The Infrared Spectra of Minerals*; Mineralogical Society of Great Britain and Ireland: London, 1974.
(35) Costanzo, P. M.; Giese, R. F.; Lipsicas, M. Static and dynamic structure of water in hydrated kaolinites. 1. The static structure. *Clays Clay Miner.* **1984**, *32*, 419−428.
(36) Amara, A. B. H. X-ray diffraction, infrared and TGA/DTG analysis of hydrated nacrite. *Clay Miner.* **1997**, *32*, 463−470.
(37) Bish, D.; et al. The first X-ray diffraction measurements on Mars. *IUCRJ* **2014**, *1*, 514−522.
(38) Goudge, T. A.; Mustard, J. F.; Head, J. W.; Salvatore, M. R.; Wiseman, S. M. Integrating CRISM and TES hyperspectral data to characterize a halloysite-bearing deposit in Kashira crater, Mars. *Icarus* **2015**, *250*, 165−187.
(39) Wray, J. J.; Murchie, S. L.; Squyres, S. W.; Seelos, F. P.; Tornabene, L. L. Diverse aqueous environments on ancient Mars revealed in the southern highlands. *Geology* **2009**, *37*, 1043−1046.
(40) Hazen, R. M.; et al. Clay mineral evolution. *Am. Miner.* **2013**, *98*, 2007−2029.

DOI: 10.1021/acsearthspacechem.9b00255
ACS Earth Space Chem. 2020, 4, 183−188